Journal of Materials Chemistry A

ROYAL SOCIETY OF CHEMISTRY

COMMUNICATION

View Article Online
View Journal | View Issue

Check for updates

Cite this: *J. Mater. Chem. A*, 2025, **13**, 18313

Received 8th April 2025
Accepted 27th May 2025

DOI: 10.1039/d5ta02769a

rsc.li/materials-a

Open Access Article. Published on 28 May 2025. Downloaded on 4/9/2026 12:22:00 PM.
This article is licensed under a Creative Commons Attribution 3.0 Unported Licence.

Breaking structural symmetry to facilitate fast reaction kinetics†

Woosik Min,‡ Seokhyun Lee,‡ Juncheol Hwang, Sangho Yoon and Duho Kim *

Breaking the intrinsic symmetry in crystal structures has emerged as a powerful strategy to enhance electrochemical reaction kinetics in advanced battery materials. In this study, we systematically investigate how introducing larger heteroatoms (*e.g.*, Se, Te) into a cubic host lattice disrupts its symmetry, thereby creating new pathways for ionic transport. By expanding and splitting bond lengths, doping weakens the local bonding environment and reduces chemical hardness, which in turn lowers the energy barriers for (de)lithiation and accelerates phase-transition kinetics. Furthermore, Li kinetic calculations reveal that the resultant lattice distortions give rise to multiple diffusion routes, including newly formed channels with notably lower migration barriers. These findings underscore the critical role of structural asymmetry in improving charging rates and mitigating voltage hysteresis. Overall, this work highlights symmetry breaking as a promising design concept for developing high-performance battery materials, offering a pathway to faster Li-ion transport.

Introduction

As global demand for electric vehicles continues to surge, the development of rechargeable battery technologies has been accelerating, driving their extensive adoption.[1–5] Despite these advancements, a number of technical challenges persist, with slow charging speeds remaining a major obstacle to widespread acceptance.[6–8] Increasing current density to achieve faster charging inevitably leads to structural degradation and voltage hysteresis, ultimately shortening cycle life and reducing energy density.[9–14] These issues underscore the need for design strategies that can improve ion transport without compromising structural integrity.

To address these challenges, a variety of materials engineering approaches have been proposed. Among them, the strategy of disrupting or breaking structural symmetry has attracted significant attention for enhancing reaction kinetics.[15–17] Such controlled disruption in cathode materials modifies the internal crystal architecture, altering (de)lithiation mechanisms and diffusion pathways—often *via* newly formed percolating networks or modified diffusion routes.[18–21] Moreover, prior theoretical studies have shown that asymmetric cation distributions at interfaces can also stabilize electrochemical phases and enhance Li-ion transport, suggesting that symmetry breaking is relevant not only in the bulk but also at the electrode–electrolyte interface.[22–24] This strategy has shown great potential for improving fast-charging capability and energy efficiency in various lithium-ion batteries.

Nevertheless, despite the promise of symmetry breaking, a comprehensive understanding of how local structural changes and reaction kinetics interact remains limited.[25–27] Further insights into this interplay are crucial for exploiting symmetry breaking to achieve faster charging rates and reduced hysteresis.[28–31] In particular, theoretical studies linking local bond distortion, chemical hardness variation, and lithium migration energy barriers are still lacking.

In this study, we investigated the impact of crystal-symmetry disruption on the structural and kinetic properties of lithium sulfide (Li_2S)—a cubic (*Fm*3*m*) material that acts as the final discharge product in lithium–sulfur batteries. By introducing larger heteroatoms such as selenium (Se) and tellurium (Te), we aimed to break the intrinsic symmetry and evaluate the resulting changes in bond lengths and diffusion pathways. Our findings reveal that structural disruption causes uniform bond lengths to diverge and increase, leading to weaker Li–S bonds. This weakening effect becomes more pronounced with increasing distortion, resulting in further separation of bond lengths and an overall reduction in chemical hardness. Such lowered chemical hardness is expected to facilitate delithiation during charge–discharge cycles, thus improving phase-transition kinetics and possibly reducing voltage hysteresis.

Department of Mechanical Engineering (Integrated Engineering Program), Kyung Hee University, 1732, Deogyeong-daero, Giheung-gu, Yongin-si, Gyeonggi-do, 17104, Republic of Korea. E-mail: duhokim@khu.ac.kr

† Electronic supplementary information (ESI) available. See DOI: https://doi.org/10.1039/d5ta02769a

‡ W. Min and S. H. Lee contributed equally to this work.

Open Access Article. Published on 28 May 2025. Downloaded on 4/9/2026 12:22:00 PM.
This article is licensed under a Creative Commons Attribution 3.0 Unported Licence.

Moreover, the disrupted crystal symmetry distorts Li_2S tetrahedra, altering Li–Li distances and splitting the previously uniform diffusion path into several distinct routes. As structural distortion increases, these routes become more differentiated, potentially decreasing migration barriers and thus enabling faster ionic kinetics. Overall, this study demonstrates that intentionally breaking structural symmetry—by modifying bond strength and diffusion pathways—can significantly enhance electrochemical performance, offering a promising strategy for future battery designs.

Results and discussion

The chemical hardness between Li and X (X = S, Se, Te) has been identified as a key factor in tuning solid-state conversion kinetics for high-energy-density lithium–sulfur batteries.[32,33] Reducing chemical hardness by doping into the host material has been shown to lower the phase transition barrier during the solid-state conversion process, from both local and macroscopic structural standpoints.[34] In other words, foreign ions can play a functional role in destabilizing the Li_2S solid-state cathode framework, thereby affecting its kinetic properties.[35] Based on these insights, we investigated in detail the correlation between the local Li–X structure and Li-ion transport. To this end, we categorized lithium sulfide models into two main groups: (i) the symmetrical Li_2S structure, and (ii) doped lithium chalcogenides exhibiting doping-induced asymmetry, both rooted in the cubic crystal system. For the former, Fig. 1a presents pristine Li_2S devoid of any heteroatom doping. Li_2S adopts a perfect cubic (*Fm*3*m*) lattice, wherein each Li atom is tetrahedrally coordinated by four S atoms. Due to this high degree of symmetry, all tetrahedra within the lattice have uniform bond lengths, forming an orderly environment for Li-ion diffusion. In this fully symmetrical arrangement, Li-ions move between equivalent tetrahedra along a consistent diffusion pathway. While this regularity allows for predictable diffusion kinetics, it also restricts the emergence of alternative Li-ion migration routes. By contrast, Fig. 1b conceptually illustrates how the Li_2S lattice would be modified by the incorporation of heteroatoms. The presence of larger or different elements induces structural distortions that disrupt the lattice symmetry, leading to variations in bond lengths, which directly influence bond strength.[36] Consequently, each Li-centered tetrahedron may experience notable distortion compared to the pristine state, giving rise to multiple new diffusion pathways. Such additional routes can help decrease the migration barrier for Li-ions, enabling faster Li-ion motion.[37] Hence, doping-induced symmetry breaking emerges as a promising strategy for improving reaction kinetics in Li-based battery materials by reshaping both the bond-length distribution and tetrahedral geometry.[38] To further elucidate the effects of asymmetry on Li kinetics, Fig. 2a and b display the crystal structures of lithium sulfide (Li_2S) doped with selenium (Se) and tellurium (Te), respectively. Because Se and Te ions are larger than the S ion, replacing the sulfur ion with these dopants naturally disrupts the initially symmetric Li_2S lattice.

In Fig. 2a, the addition of Se, which is larger than S, visibly distorts the local lattice environment, causing the tetrahedra to deviate from their symmetrical configurations. This distortion becomes even more pronounced when the larger Te atoms

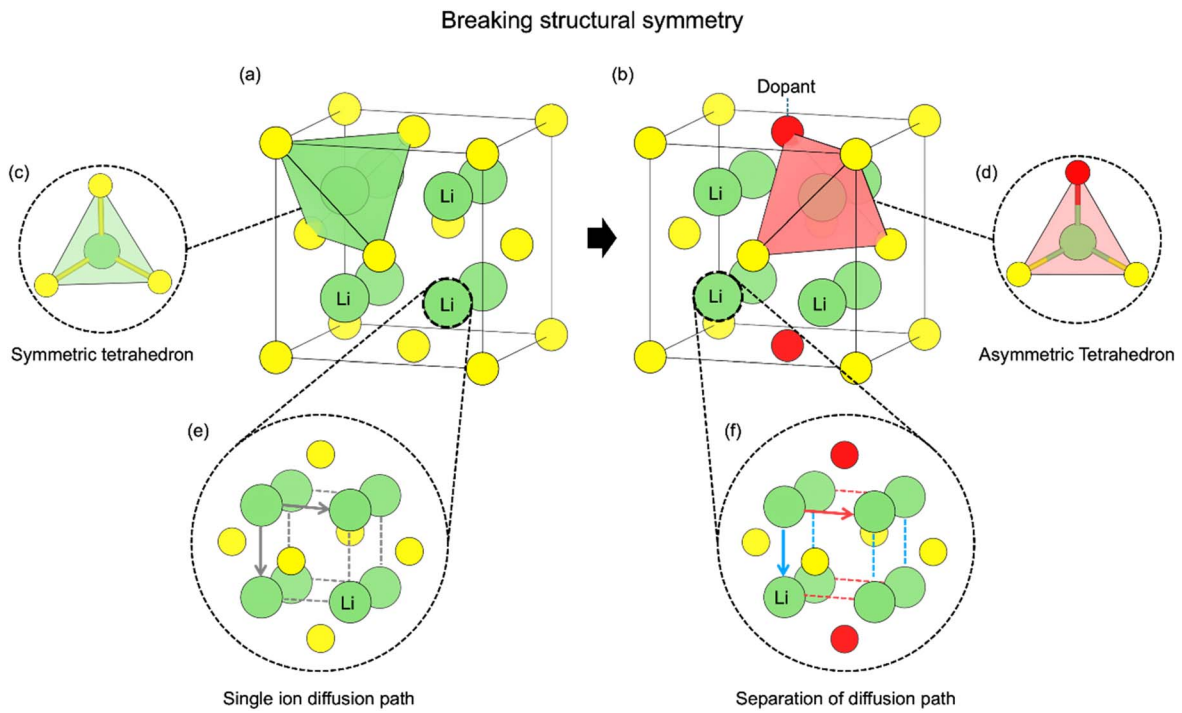

Fig. 1 Structural schematics of pristine Li_2S (a, c and e) and doped Li_2S (b, d and f) showing how heteroatom doping breaks lattice symmetry and creates multiple Li-ion diffusion pathways.

 This journal is © The Royal Society of Chemistry 2025

Open Access Article. Published on 28 May 2025. Downloaded on 4/9/2026 12:22:00 PM.
This article is licensed under a Creative Commons Attribution 3.0 Unported Licence.

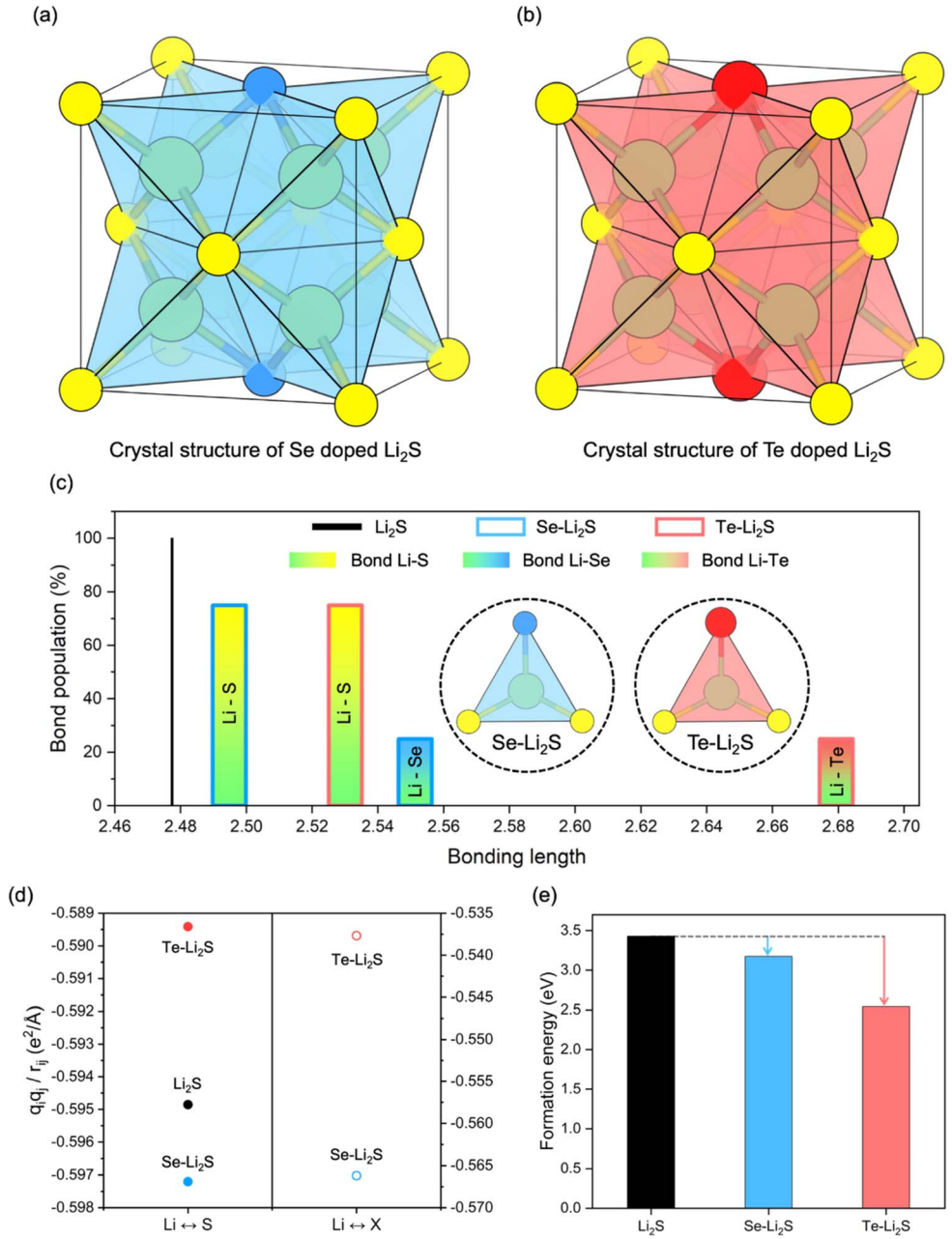

Fig. 2 Crystal structure of Se-Li_2S (a) and Te-Li_2S (b), (c) bond population of Se-Li_2S and Te-Li_2S, (d) electrostatic interaction Li–S and Li–X (X = Se, Te) in Se-Li_2S and Te-Li_2S, (e) formation energy of Li_2S, Se-Li_2S and Te-Li_2S.

(Fig. 2b) are introduced, further disturbing the original symmetry. Fig. 2c shows how substituting S with larger heteroatoms (Se or Te) affects the bond-length distributions of pristine and doped Li_2S. As summarized in Table S1,† doping expands both the total lattice volume and the volume of individual Li-centered tetrahedra. In pristine Li_2S, only a single type of bond length is observed due to its high symmetry. However, doping with Se or Te yields a new bond type—Li–X (X = Se or Te)—causing additional peaks in the bond-length distribution. Moreover, the average bond lengths for both Li–S and Li–X bonds increase upon doping, a shift that is particularly prominent in Te-doped Li_2S, implying a more intense structural distortion. This asymmetry leads to a divergence in bond lengths, altering the local coulombic interactions within the LiS_4 tetrahedra.

To investigate these effects at the electronic level, we performed Bader charge analyses on relaxed Li_2S, Se-Li_2S, and Te-Li_2S, focusing on the average net charges of Li, S, Se, and Te (see Fig. S1†). Despite the structural distortions caused by doping (split bond lengths and displaced atomic positions), the average net charges remained largely unchanged. Thus, the principal structural and electrochemical modifications appear to stem primarily from alterations in bond lengths and atomic arrangements rather than from significant charge transfer.

Open Access Article. Published on 28 May 2025. Downloaded on 4/9/2026 12:22:00 PM.
This article is licensed under a Creative Commons Attribution 3.0 Unported Licence.

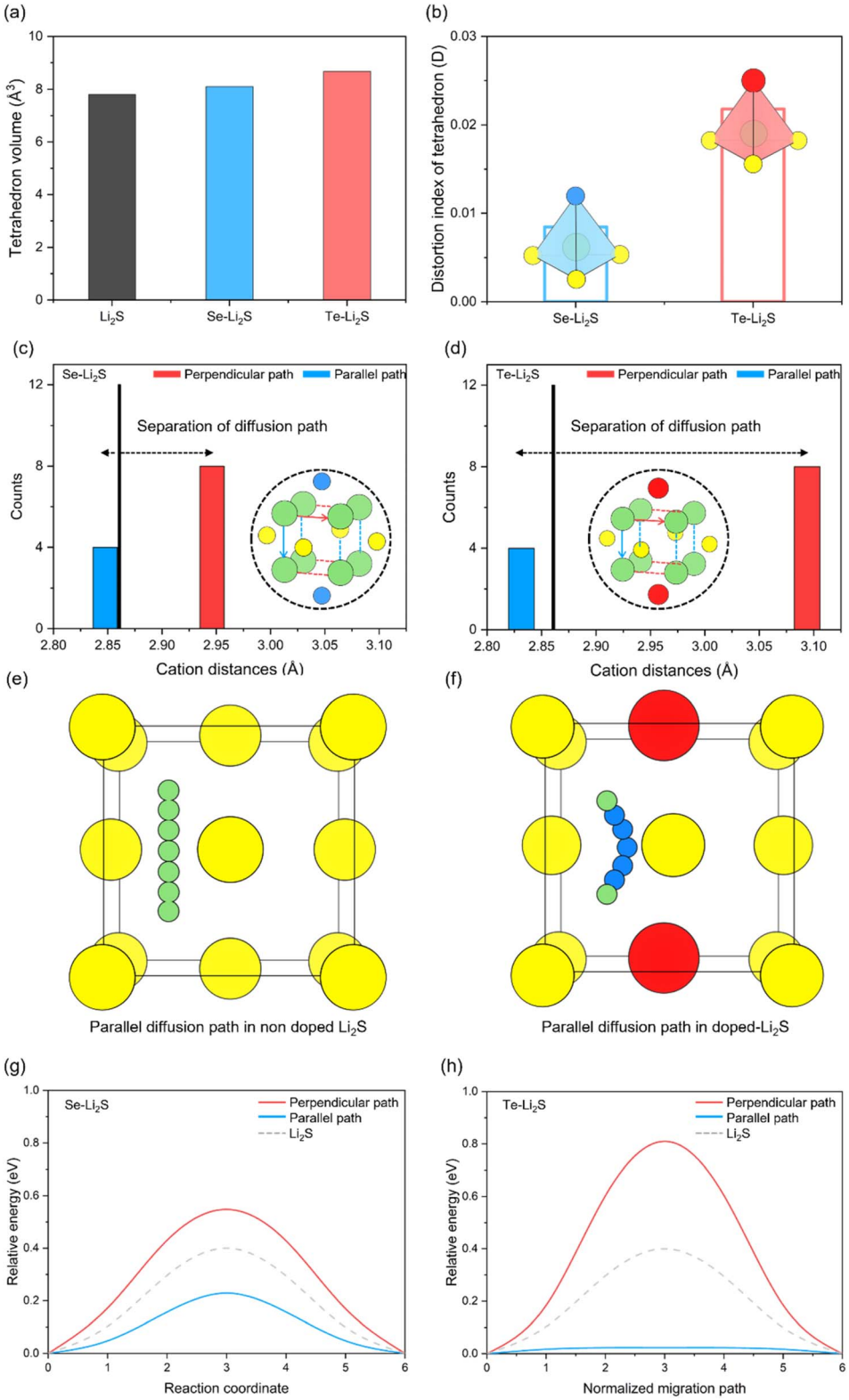

Fig. 3 (a) Tetrahedron volume of pristine Li_2S, Se-Li_2S and Te-Li_2S, (b) distortion index of tetrahedron in Se-Li_2S and Te-Li_2S, cation distance counts of Se-Li_2S (c) and Te-Li_2S (d), schematic illustration of Li diffusion path in pristine Li_2S (e) and doped Li_2S (f), calculated relative energy profiles along the parallel and perpendicular diffusion paths in Se-Li_2S (g) and Te-Li_2S (h).

 This journal is © The Royal Society of Chemistry 2025

Open Access Article. Published on 28 May 2025. Downloaded on 4/9/2026 12:22:00 PM. This article is licensed under a Creative Commons Attribution 3.0 Unported Licence.

Fig. 2d illustrates the attractive pair electrostatic interactions, estimated by the ratio $q_i q_j / r_{ij}$ (eqn (S1)†), using our calculated average bond lengths and net charges.

More negative values imply stronger chemical hardness, whereas less negative values indicate weaker chemical hardness.[32,39] The increased bond lengths in doped samples generally correspond to weaker Li–X interactions compared to pristine Li_2S, with the effect growing especially evident when involving the larger Te atom. To clarify how this bond weakening influences the (de)lithiation process, we examined the thermodynamics of lithium vacancy formation in Li_2S, Se-Li_2S, and Te-Li_2S, as shown in Fig. 2e. Structures featuring weaker bonds exhibited lower vacancy formation energies, suggesting that Li-ions can be inserted and extracted more readily, which is advantageous for improving solid-state conversion kinetics.[40,41] In Fig. 3a, the volume of each Li-centered tetrahedron is shown to increase upon doping with larger atoms such as Se or Te. This volumetric expansion stems from the dopant-induced bond-length elongation, reflecting how extended bonds directly lead to enlarged local structures. Subsequently, Fig. 3b demonstrates that rising tetrahedral volume and split bond lengths collectively result in pronounced distortion within each Li-centered unit. These deviations become especially substantial in Te-doped structures, highlighting the severe departure from the pristine cubic geometry. Fig. 3c reveals that Se doping induces a separation of Li diffusion pathways, mirroring the trend observed in the bond-length distribution. We label these newly formed routes the "parallel" path—where Li hops occur parallel to the dopant—and the "perpendicular" path—where hops take place in a perpendicular manner. Although the overall lattice volume and tetrahedral size grow, certain parallel diffusion routes in doped Li_2S become shorter than in pristine Li_2S. In other words, while most bond lengths increase, some diffusion channels may shrink or become reoriented in ways that shorten the Li–Li hopping distance. Fig. 3d shows that these phenomena intensify with larger dopants such as Te, yielding an even more significant divergence among various diffusion pathways and thus augmenting the overall structural asymmetry. Given these unexpected changes, we employed Nudged Elastic Band (NEB) calculations to quantify how the altered diffusion routes influence Li-ion migration energy barriers. Fig. 3e and f provide a schematic of these modified diffusion paths, focusing particularly on the newly formed parallel route. A more detailed description of the perpendicular path also can be found in Fig. S2.† In pristine Li_2S, Li-ion migration follows a straightforward, linear pathway due to its symmetric architecture. However, with heteroatom substitution, the broken symmetry and localized charge imbalances introduce new, more complex diffusion routes. Fig. 3g and h illustrate the NEB-calculated migration barriers for both parallel and perpendicular paths in undoped and doped Li_2S. Notably, the shorter parallel route in doped Li_2S demonstrates a markedly lower migration barrier than the path in pristine Li_2S, enabling faster Li-ion transport. Conversely, the perpendicular route—now elongated by the structural distortion—yields a higher migration barrier, inhibiting Li-ion flow relative to pristine Li_2S. This disparity becomes especially pronounced with Te doping, reflecting how substantial structural distortion drives highly divergent transport properties.

Conclusions

This work underscores the pivotal role of symmetry breaking in regulating solid-state conversion kinetics. By deliberately introducing heteroatoms (Se and Te) into the cubic Li_2S framework, we disrupt its inherent symmetry, creating new bond-length distributions and inducing notable structural distortions. This asymmetry gives rise to complex, non-linear changes in both local bonding and kinetic behavior. We find that such bond-length divergence weakens chemical hardness, thus promoting delithiation kinetics. Simultaneously, the resultant lattice distortion separates diffusion pathways, unveiling a new high-speed diffusion route with a lower migration barrier compared to undoped Li_2S. As distortion intensifies, these effects amplify, further enhancing the disparity between various diffusion paths. While larger dopants like Te produce greater structural distortion and thus more pronounced kinetic improvements, smaller dopants in specific configurations might similarly achieve these outcomes. These findings highlight that steric or electronic parameters alone cannot predict migration behavior, emphasizing the emergent nature of lattice symmetry disruption. Collectively, our findings indicate that symmetry breaking plays a crucial part in tuning both delithiation and ion-transport kinetics. We anticipate that this framework may guide future experimental and theoretical efforts in symmetry-engineered Li–S systems. Strategically introducing structural asymmetry may be extended to other lithium-based energy storage materials as a promising avenue for boosting rate performance and energy density.

Methodology

Density functional theory calculations

All computational results were obtained using the Vienna *Ab initio* Simulation Package (VASP) based on the density functional theory (DFT) method, utilizing the projector-augmented wave approach.[42] As the exchange-correlation functional, the generalized gradient approximation using the Perdew–Burke–Ernzerhof functional was employed with a plane-wave basis set based on an energy cutoff of 500 eV.[43] The total energies were sampled on a set of $4 \times 4 \times 4$ reciprocal k-point meshes generated by the Monkhorst–Pack method, and their values converged within 10^{-5} eV in total energy for electronic loops and 0.01 eV $Å^{-1}$ in interatomic forces for ionic loops. To describe Li migration path barriers, the nudged elastic band (NEB) calculations were employed with five images for linear interpolation along the diffusion paths. All calculations were conducted based on the Li diffusion path between lithium atoms among the perpendicular and parallel paths in doped-Li_2S, and the details of these paths are shown in Fig. 3e, f and S2.† The selective dynamics is used to preserve the positions of atoms in the pristine Li_2S and doped-Li_2S model which is randomly adjusted, except for moving diffusion Li^+ ion.

Open Access Article. Published on 28 May 2025. Downloaded on 4/9/2026 12:22:00 PM. This article is licensed under a Creative Commons Attribution 3.0 Unported Licence.

Data availability

The data supporting this article have been included as part of the ESI.†

Conflicts of interest

There are no conflicts to declare.

Acknowledgements

This work was supported by a grant from Kyung Hee University in 2022 (KHU-20222210).

References

1 J. Zhou, S. Qian, B. Hao, J. Liu, X. Zhou, C. Yan and T. Qian, *Adv. Funct. Mater.*, 2023, **33**, 2213966.
2 X. Wang, L. Liu, Z. Hu, C. Peng, C. Han and W. Li, *Adv. Energy Mater.*, 2023, **13**, 2302927.
3 R. He, Y. Li, Z. Yin, H. Liu, Y. Jin, Y. Zhang, H. Liu and X. Zhang, *ACS Appl. Energy Mater.*, 2023, **6**, 3903–3914.
4 M. Ahmad, T. Nawaz, I. Hussain, F. Meharban, X. Chen, S. A. Khan, S. Iqbal, P. Rosaiah, M. Z. Ansari, W. Al Zoubi and K. Zhang, *Small*, 2024, **20**, 2310099.
5 X. Huang, J. Sun, L. Wang, X. Tong, S. Xue Dou and Z. M. Wang, *Small*, 2021, **17**, 2004369.
6 Y. Chen, J. Key, K. O'Regan, T. Song, Y. Han and E. Kendrick, *Chem. Eng. J.*, 2022, **450**, 138275.
7 F. Li, R. Liu, J. Liu and H. Li, *Adv. Funct. Mater.*, 2023, **33**, 2300602.
8 M. Yuan, H. Liu and F. Ran, *Mater. Today*, 2023, **63**, 360–379.
9 H. Da, W. Fang, J. Zhu, J. Li, S. Pan, J. Li, J. Huang, H. Zhang and S. Zhang, *Small*, 2023, **19**, 2304060.
10 W. Min, T. H. Hong, J. Hwang, Y. H. Lee, J. Kee, D. J. Kim, J. T. Lee and D. Kim, *Adv. Funct. Mater.*, 2025, **35**, 2415619.
11 K. Ku, S. B. Son, J. Gim, J. Park, Y. Liang, A. Stark, E. Lee and J. Libera, *J. Mater. Chem. A*, 2022, **10**, 288–295.
12 J. P. Pender, G. Jha, D. H. Youn, J. M. Ziegler, I. Andoni, E. J. Choi, A. Heller, B. S. Dunn, P. S. Weiss, R. M. Penner and C. B. Mullins, *ACS Nano*, 2020, **14**, 1243–1295.
13 X. G. Yang and C. Y. Wang, *J. Power Sources*, 2018, **402**, 489–498.
14 T. H. Hong, W. Min, G. Choi, J. D. Kim, J. T. Lee and D. Kim, *Adv. Energy Mater.*, 2023, **13**, 2300636.
15 J. Zhang, W. Li, J. Yang, J. Wang, Q. Dong, X. Wang, Y. Wu, Y. Ren and X. Li, *Small*, 2024, **20**, 2401443.
16 S. Zhang, Z. Yang, Y. Lu, W. Xie, Z. Yan and J. Chen, *Adv. Energy Mater.*, 2024, **14**, 2402068.
17 Y. Zheng, H. Xie, J. Li, K. S. Hui, Z. Yu, H. Xu, D. A. Dinh, Z. Ye, C. Zha and K. N. Hui, *Adv. Energy Mater.*, 2024, **14**, 2400461.
18 Y. Shirazi Moghadam, S. Dinda, A. El Kharbachi, G. Melinte, C. Kübel and M. Fichtner, *Chem. Mater.*, 2022, **34**, 2268–2281.
19 Y. Sun, S. Jiao, J. Wang, Y. Zhang, J. Liu, X. Wang, L. Kang, X. Yu, H. Li, L. Chen and X. Huang, *J. Am. Chem. Soc.*, 2023, **145**, 11717–11726.
20 M. D. Radin, S. Hy, M. Sina, C. Fang, H. Liu, J. Vinckeviciute, M. Zhang, M. S. Whittingham, Y. S. Meng and A. Van der Ven, *Adv. Energy Mater.*, 2017, **7**, 1602888.
21 T. H. Hong, J. Kee, H. Jang, D. Kwon, D. Kim and J. T. Lee, *J. Alloys Compd.*, 2023, **948**, 169789.
22 Z. M. Xu, S. H. Bo and H. Zhu, *ACS Appl. Mater. Interfaces*, 2018, **10**, 36740–36747.
23 Z. Wang, Q. Su, H. Deng and Y. Fu, *ChemElectroChem*, 2015, **2**, 1001–1007.
24 X. Lei, K. Yu, R. Qi and Z. Zhu, *Chem. Eng. J.*, 2018, **354**, 1000–1009.
25 M. Z. Bazant, *Acc. Chem. Res.*, 2013, **46**, 1144–1160.
26 A. Van Der Ven, J. Bhattacharya and A. A. Belak, *Acc. Chem. Res.*, 2013, **46**, 1216–1225.
27 K. J. Jun, Y. Chen, G. Wei, X. Yang and G. Ceder, *Nat. Rev. Mater.*, 2024, **9**, 887–905.
28 A. Gao and L. Gu, *Adv. Funct. Mater.*, 2025, **35**, 2409372.
29 R. A. House, U. Maitra, M. A. Pérez-Osorio, J. G. Lozano, L. Jin, J. W. Somerville, L. C. Duda, A. Nag, A. Walters, K. J. Zhou, M. R. Roberts and P. G. Bruce, *Nature*, 2019, **577**, 502–508.
30 Q. Wu, Y. Ma, S. Zhang, X. Chen, J. Bai, H. Wang and X. Liu, *Small*, 2024, **20**, 2404660.
31 T. H. Hong, J. Y. Kee, D. Kwon, S. Park, D. Kim and J. T. Lee, *ACS Appl. Energy Mater.*, 2022, **5**, 12583–12591.
32 S. Qi, C. Li, J. Wang, X. Song, M. Zhao and G. Chen, *J. Phys. Chem. Lett.*, 2023, **14**, 7992–7999.
33 F. Liang, S. Wang, Q. Liang, A. Zhong, C. Yang, J. Qian, H. Song and R. Chen, *Adv. Energy Mater.*, 2024, **14**, 2400111.
34 J. Feng, C. Shi, X. Zhao, Y. Zhang, S. Chen, X. Cheng and J. Song, *Adv. Mater.*, 2024, **36**, 2401447.
35 K. Zhang, Z. Zhao, H. Chen, Y. Pan, B. Niu, D. Long and Y. Zhang, *Small*, 2024, **20**, 2409674.
36 C. Huang, J. Yu, C. Y. Zhang, Z. Cui, R. He, L. Yang, B. Nan, C. Li, X. Qi, X. Qi, J. Li, J. Y. Zhou, O. Usoltsev, L. Simonelli, J. Arbiol, Y. J. Lei, Q. Sun, G. Wang and A. Cabot, *Angew. Chem., Int. Ed.*, 2024, **63**, e202420488.
37 B. Lama, A. L. Smirnova and T. R. Paudel, *ACS Appl. Energy Mater.*, 2023, **6**, 10424–10431.
38 S. H. Park, N. K. Lee, S. G. Lee, J. H. Han and Y. J. Lee, *ACS Appl. Energy Mater.*, 2023, **6**, 11355–11374.
39 T. Maihom, J. Sittiwong, M. Probst and J. Limtrakul, *Phys. Chem. Chem. Phys.*, 2022, **24**, 11645–11656.
40 Y. Chu, Y. Mu, L. Zou, Y. Hu, S. Kang, H. Ren, M. Han, Q. Zhang, L. Wei and L. Zeng, *Small Struct.*, 2024, **5**, 2300247.
41 H. Wu, H. Jiang, Y. Yang, C. Hou, H. Zhao, R. Xiao and H. Wang, *J. Mater. Chem. A*, 2020, **8**, 14498–14505.
42 J. Hafner, *J. Comput. Chem.*, 2008, **29**, 2044.
43 J. P. Perdew, K. Burke and M. Ernzerhof, *Phys. Rev. Lett.*, 1996, **77**, 3865.

 This journal is © The Royal Society of Chemistry 2025